

Influence of Anisotropic Conductivity on EEG Source Reconstruction: Investigations in a Rabbit Model

Daniel Güllmar*, Jens Haucisen, *Member, IEEE*, Michael Eiselt, Frank Gießler, Lars Flemming, Alfred Anwander, Thomas R. Knösche, Carsten H. Wolters, Matthias Dümpelmann, David S. Tuch, and Jürgen R. Reichenbach

Abstract—The aim of our work was to quantify the influence of white matter anisotropic conductivity information on electroencephalography (EEG) source reconstruction. We performed this quantification in a rabbit head using both simulations and source localization based on invasive measurements. *In vivo* anisotropic (tensorial) conductivity information was obtained from magnetic resonance diffusion tensor imaging and included into a high-resolution finite-element model. When neglecting anisotropy in the simulations, we found a shift in source location of up to 1.3 mm with a mean value of 0.3 mm. The averaged orientational deviation was 10 degree and the mean magnitude error of the dipole was 29%. Source localization of the first cortical components after median and tibial nerve stimulation resulted in anatomically verified dipole positions with no significant anisotropy effect. Our results indicate that the expected average source localization error due to anisotropic white matter conductivity is within the principal accuracy limits of current inverse procedures. However, larger localization errors might occur in certain cases. In contrast, dipole orientation and dipole strength are influenced significantly by the anisotropy. We conclude that the inclusion of tissue anisotropy information improves source estimation procedures.

Index Terms—Animal model, anisotropic conductivity, DTI, EEG, FEM, source localization.

I. INTRODUCTION

SOURCE localization based on electroencephalography (EEG) data estimates neuronal activity with the help of a source model (commonly a current dipole) and a volume conductor model. Since the volume conductor model represents the conductivity distribution in the head it, therefore, requires knowledge about tissue conductivities. The conductivity is known to be anisotropic (in particular in white matter structures) [1]–[6]. However, this property is usually neglected because an *in vivo* determination of anisotropy has not been available until recently. Magnetic resonance diffusion tensor imaging (DTI) provides the key to extract this conductivity tensor information individually [7], [8]. With this technique the conductivity tensors are not measured directly but rather inferred from the diffusion tensors using a model [8] which describes the movement of both water molecules and electrically charged particles (ions). Hence, DTI yields anisotropic conductivity information. Application of finite-element method (FEM), which has been used for more than two decades in the field of EEG source localization [9]–[12], makes it then possible to include this anisotropic conductivity information into the modeling.

The question then arises how the neglect of anisotropic conductivity (which has been basically done until now) influences the electric surface potential and source localization in EEG experiments. First studies in humans indicated that both the electric surface potential (forward solution) [7], [13] and the source localization (inverse solution) [14]–[17] are affected. However, the practicality to perform such studies in humans, despite being highly important, is rather limited. Specifically, direct invasive evaluation of source localization is difficult and the functional and anatomical variability is high. Therefore, animal models have always been important in neuroscience, and source localization studies have also been performed recently in animals [18]–[21].

In this paper, we investigated the influence of anisotropic white matter tissue conductivity on EEG based forward and inverse solutions in the rabbit. Additionally, we took advantage of the precise anatomical knowledge available for the rabbit and the possibility to perform invasive procedures in order to validate our software and simulations with the help of measurements.

Manuscript received August 7, 2005; revised February 19, 2006. This work was supported in part by the German Ministry of Science, in part by the European Union, in part by the German Research Council (DFG), and in part by the Interdisciplinary Center for Clinical Studies (IZKF), Jena (TP 1.8). *Asterisk indicates corresponding author.*

*D. Güllmar is with the Biomagnetic Center, Department of Neurology, and Medical Physics Group, Institute of Diagnostic and Interventional Radiology, Erlanger Allee 101, 07747 Jena, Germany (e-mail: daniel.guellmar@med.uni-jena.de).

J. Haucisen was with the Biomagnetic Center, Department of Neurology, 07747 Jena, Germany. He is now with the Institute of Biomedical Engineering and Informatics, Technical University Ilmenau, 99893 Ilmenau, Germany (e-mail: jens.haucisen@tu-ilmenau.de).

M. Eiselt is with the Institute of Pathological Physiology, FSU Jena, Jena 07747, Germany (e-mail: Michael.Eiselt@mti.uni-jena.de).

F. Gießler is with the Biomagnetic Center, Department of Neurology, FSU Jena, Jena 07747, Germany (e-mail: giessler@biomag.uni-jena.de).

L. Flemming was with the Biomagnetic Center, Department of Neurology, FSU Jena, Jena 07747, Germany.

A. Anwander and T. R. Knösche are with the Max-Planck Institute of Human Cognitive and Brain Science, 04103 Leipzig, Germany (e-mail: anwander@cbs.mpg.de; knoesche@cbs.mpg.de).

C. H. Wolters is with the Institute of Biomagnetism and Biosignalanalysis, University Münster, Münster 48149, Germany (e-mail: carsten.wolters@uni-muenster.de).

M. Dümpelmann is with eemagine Medical Imaging Solutions GmbH, 12489 Berlin, Germany (e-mail: Matthias.Duempelmann@eemagine.com).

D. S. Tuch is with the Massachusetts General Hospital, Charlestown, MA 02129 USA.

J. R. Reichenbach is with the Medical Physics Group, Institute of Diagnostic and Interventional Radiology, FSU Jena, Jena 07743, Germany (e-mail: juergen.reichenbach@med.uni-jena.de).

Color versions of Figs. 1–9 are available online at <http://ieeexplore.ieee.org>.

Digital Object Identifier 10.1109/TBME.2006.876641

This paper presents three different studies with the aim to quantify the influence of anisotropy:

In the first study (*study I*) we investigate the influence of white matter anisotropy measured with DTI in the forward and inverse calculation of focal sources. For this purpose we employ two different types of volume conductors: 1) with isotropic conductivity; 2) with anisotropic conductivity in white matter. For the forward computations the distribution of the electrical potential computed with model 1 and 2 are compared. For the inverse computations model 1 is used, with the forward computations from model 2.

Since the results obtained in the first study were relatively complex, we analyze the effects observed in *study I* in more detail in the second study (*study II*). The irregularly shaped white matter compartment of the rabbit was replaced by an artificial cube of anisotropic conductivity tensors. This cube, due to its regular geometrical structure, allows us to quantify how the mutual interdependencies between dipole positions and orientations, location and orientation of the gray-white matter interface, and the orientation of the anisotropic conductivity influence the forward and inverse solutions. To test these influences on multiple dipoles briefly, we have chosen three dipole positions selected from *study II* and performed a forward simulation with combinations of these dipoles (*study III*). The last study provides a validation of the simulations by means of source reconstruction based on measured electrocorticogram (ECoG) data.

II. MATERIALS AND METHODS

A. MRI

T1-weighted, high-resolution as well as a diffusion weighted tensor MRI data were acquired at 1.5 T in a White New Zealand rabbit during a single session by using a surface coil (Siemens Magnetom Vision, Siemens Medical Systems, Germany, Erlangen). The T1-weighted data set was obtained by employing a three-dimensional (3-D), RF-spoiled FLASH gradient echo sequence with TR/TE 40/11 ms and 204 slices with an isotropic resolution of 0.625 mm³. For the diffusion tensor scan we employed an interleaved Turbo-STEAM sequence [22] with TR/TE 15614/68 ms, b-value 500 s/mm², 20 slices, 16 averages with 1 × 1 × 2 mm³ voxels. The diffusion gradients were oriented in six noncollinear directions and one null image was acquired in order to normalize for nondiffusion attenuation. The diffusion scan was acquired twice in an interleaved manner to obtain overall 40 slices, which covered the head of the rabbit completely. Since the high-resolution, anatomic scan was run in sagittal orientation and the diffusion scan in coronal orientation, an additional low-resolution 3-D, T1-weighted data set with the same location and orientation as the diffusion scan was acquired (TR/TE 600/14 ms, 0.5 × 0.5 mm² in-plane resolution, 4-mm slice thickness). The high-resolution sagittal data set was then co-registered to the low-resolution coronal data set by employing SPM2 [23].

B. Model Construction

The co-registered high-resolution T1 weighted data set was semi-automatically segmented (Curry, Neuroscan, Ster-

ling, VA). The outermost surface (skin) and the outer brain boundary were determined with the help of a region-growing algorithm. The outer skull boundary was obtained by dilating the outer brain boundary. In order to ensure a closed 3-D skull layer we used a minimum thickness of one discretization step (0.6 mm). White matter volume was determined by applying a threshold-based, region-growing segmentation. The FEM model included 662 937 nodes with cubic elements (element length = 0.6 mm). The isotropic conductivities were set to $\sigma = 0.33$ S/m (skin), $\sigma = 0.0042$ S/m (skull), $\sigma = 0.337$ S/m (gray matter), and $\sigma_{\text{iso}} = 0.14$ S/m (white matter). For the anisotropic FEM, we assigned anisotropic conductivity tensors to all volume elements, which belonged to white matter. In the isotropic FEM, we used isotropic conductivity with isotropic tensors instead of using scalars. Following the proposition of Basser *et al.* [24], we assumed that the conductivity tensors have the same alignment as the measured diffusion tensors, i.e., they share the eigenvectors with the diffusion tensors. Shimony *et al.* [25], who measured diffusion anisotropy in 12 regions of interest in human white and gray matter, have shown that in commissural, projection and also association white matter, the shape of the diffusion ellipsoids is strongly prolate ("cigar-shaped"), whereas gray matter was found to be closely isotropic. Therefore, we assumed prolate rotationally-symmetric tensor-ellipsoids for the white matter compartment and modeled the conductivity tensor σ for a white matter finite element as

$$\sigma = \mathbf{S} \begin{pmatrix} \sigma_{\text{long}} & & \\ & \sigma_{\text{trans}} & \\ & & \sigma_{\text{trans}} \end{pmatrix} \mathbf{S}^{-1} \quad (1)$$

where \mathbf{S} is the orthogonal matrix of unit length eigenvectors of the measured diffusion tensor at the barycenter of the white matter finite element and σ_{long} and σ_{trans} are the eigenvalues parallel (longitudinal) and perpendicular (transverse) to the fiber directions, respectively, with $\sigma_{\text{long}} \geq \sigma_{\text{trans}}$. Given the lack of direct measurements of white matter conductivity anisotropy in the rabbit brain, we started from the isotropic conductivity value of $\sigma_{\text{iso}} = 0.14$ S/m and simulated the anisotropic case in the following way: For a given anisotropy ratio of $\sigma_{\text{long}} : \sigma_{\text{trans}}$ equal to 10:1, we calculated the longitudinal and the transverse eigenvalues by obeying the so-called volume constraint [14], which retains the geometric mean of the eigenvalues and, thus, the volume of the conductivity tensor, i.e.,

$$\frac{4}{3}\pi\sigma_{\text{iso}}^3 = \frac{4}{3}\pi\sigma_{\text{long}}\sigma_{\text{trans}}^2 \quad (2)$$

For the forward problem, we used a standard variation procedure in order to transform the Poisson-like elliptic differential equation for the electric potential from the quasi-static Maxwell equations into an algebraic system of linear equations [26]. To model the primary current in the FEM [27], we used a "distributed dipole," which has been previously described and intensively validated [26], [28]. We solved the resulting high-resolution linear equation system, which has a large but sparse symmetric system matrix by means of an iterative algebraic multigrid preconditioned conjugate gradient

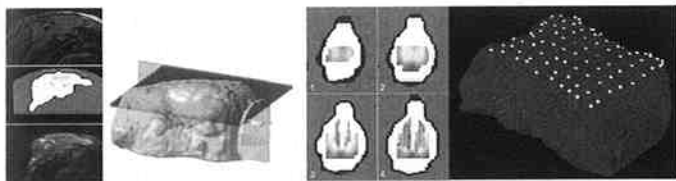


Fig. 1. Overview of the setup for the forward simulation with measured conductivity tensors. The left column shows sagittal slices of the MRI 3-D FLASH scan, the segmentation result including four compartments (skin, bone, gray matter, and white matter), and a diffusion weighted image of the DTI scan. The second column shows a 3-D model of the isosurface of the rabbit model which indicates the position of the sagittal slices in column one and the position of the four axial planes in which the dipole source space was located. The third column shows the four numbered (1–4) axial slices in which the dipoles were placed for the simulation. The dipole source space is color coded indicating the distance to the anisotropic tissue (yellow=close; red=distant). The fourth column shows the FEM model of the rabbit including the position of the 100 electrodes.

method (AMG-CG), which was parallelized for distributed memory computers. The outstanding performance of the AMG preconditioner in comparison with other methods has been demonstrated previously [26], [29]. The AMG approach is especially suitable for anisotropic problems and its stability has been shown by Wolters *et al.* [26]. For an efficient solution of the inverse problem, we exploited a FE lead field basis approach [30], [31], which dramatically reduces the complexity of the computations and allows to perform the extensive inverse simulation studies in an acceptable time. All forward and inverse computations were performed with the software developed in the SimBio project [32] including the Inverse Toolbox and the FE tool NeuroFEM [33].

C. Electric Measurements

Cortical somatosensory potentials were evoked by electric stimulation of the median and the tibial nerve (0.5 mA constant current square wave pulses, inter-stimulus interval 500 ms) on a 6 months old White New Zealand rabbit. The rabbit was anaesthetized (Ketamin 24–30 mg/kg per h and Xylazin 2.4–3 mg/kg per h), kept normothermic and was allowed to breathe spontaneously. Small silver stimulation electrodes were placed on the right median and right tibial nerve. After removing of the skin and skull bone ECoG (Neuroscan Synamps, El Paso, TX) was recorded by using a grid of 4×4 electrodes over the left hemisphere. The diameter of each single electrode was 0.25 mm and spatial distance between adjacent electrodes was 1.25 mm. Data were recorded with a sampling rate of 2 kHz, a high-pass filter of 0.3 Hz and a low-pass filter of 300 Hz. 2048 trials were averaged. The position of the electrodes in relation to the somatosensory cortex was determined. The experiments were approved by the Ethics Committee of the State of Thuringia, Germany.

D. Forward Simulations

1) *Study I: Conductivity Tensors Derived From DTI:* The conductivity tensors of the rabbit's white matter, as derived from DTI measurements, were used in the anisotropic model. We calculated the electric potential produced by 1360 cortically located dipoles (1 mm spacing) for both radial and tangential orientation (with respect to the skull) at 100 electrode positions on the rabbit skin (Fig. 1).

The positions of the electrodes were arranged in such a way as to cover the dipolar potential distribution for each dipole position and orientation, which occurred in the study. The dipoles were placed only in gray matter with a minimum distance of 1 mm to the skull and to the white matter. The forward computed data obtained with the isotropic and anisotropic model were analyzed by calculating relative difference measure (RDM*) values and magnitude difference (MAG) values of the electrical potential maps for each single dipole and each orientation. RDM* and MAG were calculated according to Meijs *et al.* [34] as follows:

$$\text{RDM}^* = \sqrt{\sum_{i=1}^n \left(\frac{\text{ref}_i}{\sqrt{\sum_{j=1}^m \text{ref}_j^2}} - \frac{\text{meas}_i}{\sqrt{\sum_{j=1}^m \text{meas}_j^2}} \right)^2} \quad (3)$$

$$\text{MAG} = \sqrt{\frac{\sum_{i=1}^m \text{meas}_i^2}{\sum_{i=1}^m \text{ref}_i^2}} \quad (4)$$

Thereby, the values obtained with the isotropic model were interpreted as measurement (meas) and the values obtained with the anisotropic model were used as reference (ref). The indices j and i represent the number of the electrodes used in the setup. RDM* as well as MAG values were then represented as color-coded maps in the dipole source space, where 4 axially cut planes were used (Fig. 1). The MAG value, which occurs in the forward analysis and the dipole magnitude change (MC), which is computed in the inverse analysis, are typically around unity, so that values below one indicate a decrease and values above one represent an increase of the variables MAG and MC. Since the ranges of values below and above unity into which MAG and MC are mapped are different, therefore making a statistical analysis difficult, we introduced an unsigned MAG_{rel} in the forward analysis and an unsigned relative magnitude change (MC_{rel}) in the inverse analysis. These latter quantities were calculated according to (5) and (6), respectively

$$\text{MAG}_{\text{rel}} = \left| 1 - \frac{\sqrt{\sum_{i=1}^n \text{meas}_i^2}}{\sum_{i=1}^n \text{ref}_i^2} \right| \quad (5)$$

$$\text{MC}_{\text{rel}} = \left| \frac{\text{magnitude}_{\text{original}} - \text{magnitude}_{\text{inverse}}}{\text{magnitude}_{\text{original}}} \right| \quad (6)$$

2) *Study II: Artificial Anisotropic Cube:* In order to obtain more specific information about the influence of anisotropic conductivity we replaced the experimental derived conductivity tensors by an artificial cube of anisotropic conductivity (dimension $12 \times 12 \times 12 \text{ mm}^3$) in the rabbit brain (Fig. 2). The anisotropy ratio in the cube was set to a ratio of 10:1:1 ($\sigma_{\text{long}} = 0.65 \text{ S/m}$ and $\sigma_{\text{trans}} = 0.065 \text{ S/m}$) in left-right orientation. A total of 4104 single dipoles were placed around this cube in 3 layers. For each dipole location all three independent orientations (with respect to the orientation of the anisotropy within the artificial cube) were considered [Fig. 2(d)–(f)], i.e., we used dipoles oriented in anterior-posterior (AP), left-right

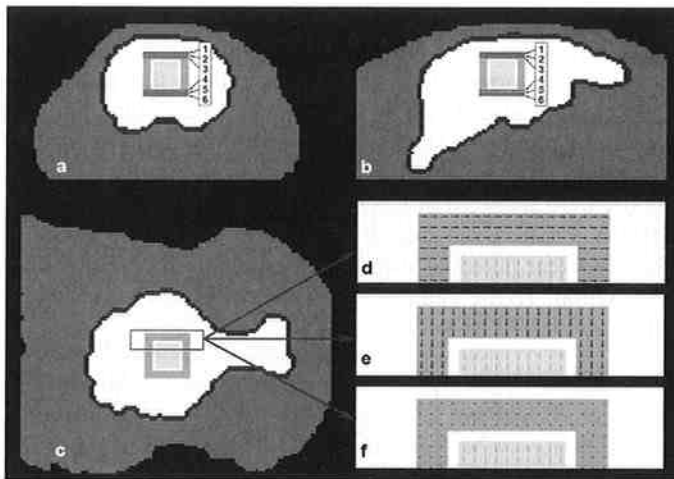


Fig. 2. Schematic view of the positioning of the artificial anisotropic cube (light gray) employing the segmented rabbit model. Subfigures (a)–(c) show a coronal, sagittal and axial slice, respectively. In (a) and (b), the positions of the planes which were used for demonstration of the results (number 1–6) are shown. (d) and (e) Zoomed view of the axial slice in subfigure c and demonstrate the positioning and orientation of the dipoles as well as the conductivity tensors in the anisotropic cube used for the forward analysis—(d) dipoles in anterior-posterior (AP) direction—(e) dipoles in the LR direction—(f) dipoles in the IS direction. The full dipole source space is indicated by blue color.

(LR), and inferior-superior (IS) direction. The electrical potential was computed at the same 100 electrodes as in study I and the forward computed data were compared analogously. The RDM* and MAG values were represented as color-coded maps in the dipole source space above and below the cube (Fig. 4).

3) *Study III: Multiple Dipoles*: The investigation of the influence of anisotropic conductivity to the forward solution in EEG using multiple dipoles leads to a vast number of possible spatial as well as directional dipole arrangements. Therefore, we selected one source position from the dipoles of the AP, LR, and IS data sets, respectively, which were used in study II and showed the largest RDM* within their respective data sets. The maximum RDM* for the AP oriented dipoles was found on the right hand side of the block, for the LR oriented dipoles below the block and for the IS oriented dipoles also at the right hand side of the block. The distance between the two AP and IS oriented dipoles was 1.3 mm, their distances to the LR dipole were 8.05 and 7.42 mm, respectively. We performed forward simulation with the combination of two dipoles (AP + LR, AP + IS, LR + IS) and all three dipoles (AP + LR + IS).

E. Source Localization From Simulations

To examine the influence of white matter anisotropy on source localization we employed the forward computed electric potential data, which were obtained from the anisotropic model for 4104 single dipoles separately, and reconstructed a single dipole from each simulated distribution of the electric potential using the isotropic model. The Simplex algorithm from the SimBio Inverse Toolbox (IP) was applied to solve the non-linear optimization problem [14]. The initial guess for source localization was located at an average distance of 1 mm from the position of the original dipole, which was used to compute the forward solution. Such an initial guess should minimize

the effect of local minima in the goal function. The resulting dipole positions, orientations, and strengths were compared to the corresponding original dipole parameters and the changes (dipole shift, orientation change, and magnitude change) were visualized as color-coded maps in the dipole source space, similar to the comparison of the forward solutions described above. Source localization was performed separately for *study I* and *II*.

F. Source Localization From Measurements

Based on the 16 channel ECoG measurements we reconstructed the dipolar source evoking the potential map at the peak of the first cortical answer (P1, see Fig. 10) following stimulation of both the median or tibial nerve. Since the electrodes were located directly on the cortex, we used only the representation of gray and white matter for source localization with the isotropic and anisotropic FEM model (consisting of 40 902 elements). Additionally, we crosschecked our localization results with a boundary element method (BEM) model comprising only the outer surface of the brain (one compartment model) with 4000 elements. The BEM grid was generated using Curry (Compumedics, Neuroscan, El Paso, TX) and the inverse solution was performed employing also the Simbio Toolbox, which uses the Isolated Problem Approach [34], [35]. The optimization was performed using the Simplex algorithm.

G. Statistics

To derive the mean and the variance of the distributions of the calculated quantities (RDM*, MAG_{rel}, dipole shift, magnitude change (MC_{rel}), orientation change) we assumed a Rayleigh distribution, which fits to the derived distributions. The Rayleigh distribution is a special case of the Weibull distribution and their probability density function is defined by

$$f(x, b) = \frac{x}{b^2} e^{\left(\frac{-x^2}{2b^2}\right)}. \quad (7)$$

For interpretation of the data the parameter b from (7) was fitted by finding the maximum-likelihood of parameter b using

$$b = \sqrt{\frac{1}{2n} \sum_{i=1}^n x_i^2}. \quad (8)$$

The mean and the variance were calculated according to

$$\text{mean}_{\text{rayleigh}} = b\sqrt{\pi/2} \quad (9)$$

$$\text{var}_{\text{rayleigh}} = \frac{4 - \pi}{2} b^2. \quad (10)$$

III. RESULTS

A. Forward Simulations

1) *Study I: Conductivity Tensors Derived From DTI*: Fig. 3 shows the results of the RDM* and MAG mapping, which was obtained from the comparison of the forward computation for the isotropic and anisotropic rabbit head model. As can be seen the histograms clearly show non-Gaussian distributions. The

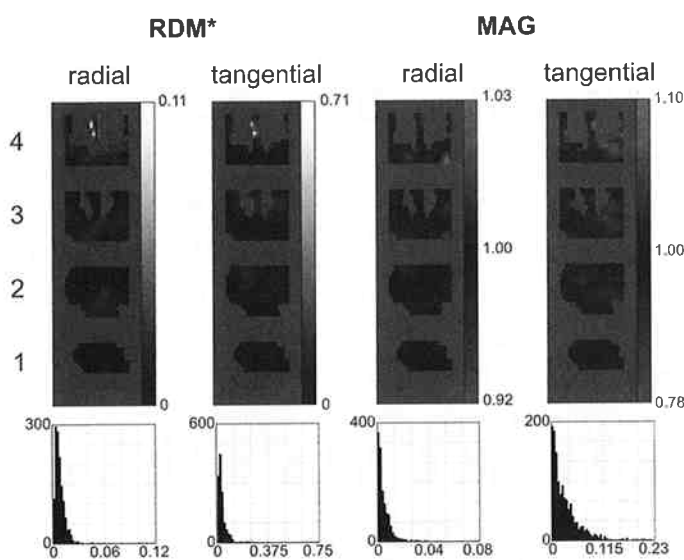


Fig. 3. Mapping of the RDM* and MAG values obtained in study I in the dipole source space for the radial and tangential dipoles. Note, that the color maps of the MAG values are not equidistant for values below and above one. Below the maps, the corresponding histograms are given, where the MAG analysis shows the relative MAG value according to (5).

mean values for RDM* and MAG_{rel} in case of radial dipoles are $1.046 \pm 0.003 \cdot 10^{-2}$ and $0.733 \pm 0.002 \cdot 10^{-2}$, respectively, and in case of tangential dipoles $5.68 \pm 0.09 \cdot 10^{-2}$ and $4.06 \pm 0.05 \cdot 10^{-2}$. It is also clear from Fig. 3 that with closer spacing of the dipoles to the white matter, the RDM* and MAG values are more deviating. The largest RDM* and MAG values are found between anisotropic segments (cut plane 4 in the dipole source space). In general the MAG/RDM^* values were larger for tangential dipoles in comparison to radial oriented dipoles. This indicates that the electric potential distribution of tangential dipoles is more influenced by anisotropy than the one of radial dipoles.

2) *Study II: Artificial Anisotropic Cube*: Fig. 4 displays the RDM* and MAG values of six transverse slices above (1–3) and below (4–6) the artificial anisotropic cube (cf. Fig. 2). The RDM* between the potential maps calculated with and without anisotropy was less than 0.02. The maximum RDM* value for the AP, LR, and IS oriented dipoles were 0.0099, 0.0073, and 0.019, respectively. The positions of these dipoles were used as source positions for the multiple dipole tests in *study III*. The RDM* values are very low with respect to the theoretical maximum of 2, whereas 2 means the compared signals are equal but with opposite sign. The values for MAG range from 0.94 to 1.04. Despite this relatively weak influence of the anisotropy, Fig. 4 nevertheless clearly demonstrates that the quantities depend on the distance between the source and the anisotropic tissue. Furthermore, the dipoles located below the anisotropic cube were more influenced than the dipoles above the cube. On the RDM* maps the strongest influence is seen close to the corners of the anisotropic cube for the two orthogonally oriented dipoles. The MAG maps show that the strongest influence of anisotropy is to be expected mainly central to areas of anisotropic tissue. It is also quite interesting to note that the MAG and RDM* values appear to be spatially decoupled: with high RDM* values the corresponding MAG values are high

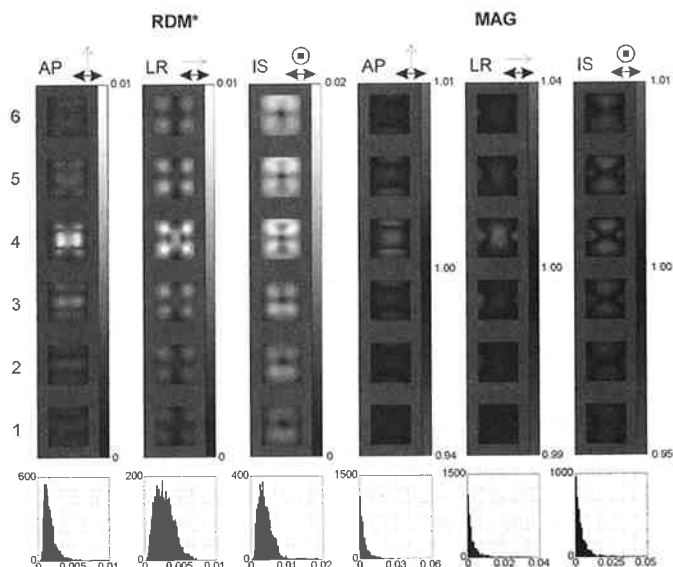


Fig. 4. Mapping of the RDM* and MAG values obtained in *study II* (anisotropic cube) in the dipole source space for dipoles in the AP (anterior-posterior), LR (left-right), and IS direction. The arrows above the maps indicate the orientation of the dipoles and the main direction of the anisotropy. Note, that the scale of the color map of the MAG values is not equidistant for values below and above one. The histograms of the MAG analysis show the relative MAG value according to (5).

or low and vice versa. Again, the histograms in Fig. 4 show a non-Gaussian distribution.

3) *Study III: Multiple Dipoles*: For the combination of multiple dipoles we obtained a RDM* and a MAG of 0.0356 and 1.001 for the AP + LR pair, 0.0137 and 0.970 for the AP + IS pair and 0.0215 and 1.0121 for the combination LR + IS. Using all three dipoles as a sources simultaneously we derived a RDM* of 0.0449 and a MAG value of 0.993. Except for the AP + LR combination all RDM* values are higher than the values obtained for a single dipole. The MAG values did not exceed the limits found in *study II*.

B. Source Localization From Simulations

1) *Study I: Conductivity Tensors Derived From DTI*: All dipoles were shifted in their location and changed their orientation due to the different volume conductor models, which were used for the forward and inverse solution. Shifts up to 0.84 mm and 1.26 mm were obtained for radial and tangential dipoles, respectively, with a mean value of 0.26 mm (radial: 0.24 mm; tangential: 0.28 mm). The mean deviation of the dipole's orientation was 10.32° (radial: 13.75° ; tangential: 4.92°) and the mean absolute magnitude change of the dipole was 28.8% (radial: 21.0%; tangential: 34.9%). In Fig. 5, the dipole shift and the changes in dipole magnitude and orientation are mapped onto the segmented slices of the rabbit's brain (see Fig. 1). Similar to the results of the forward solution (Fig. 3), the changes due to anisotropy are largest close to the anisotropic white matter.

2) *Study II: Artificial Anisotropic Cube*: The forward computed electric potential data obtained from the dipoles in the model with the artificial anisotropic cube were used to perform source localization with the model containing the isotropic cube. Fig. 6 shows the resulting dipole shift, dipole magnitude, and orientation change in six transverse slices above and below the

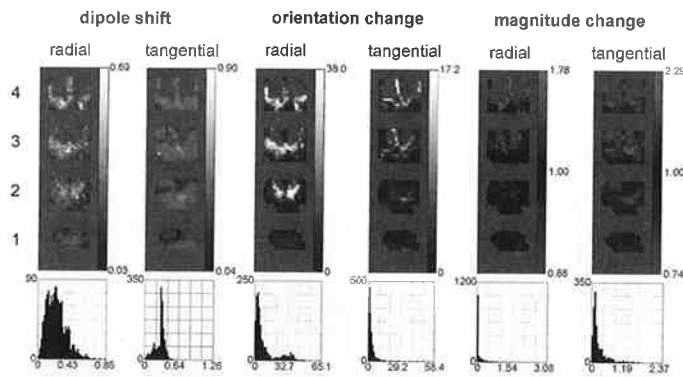


Fig. 5. Mapping of the shift, orientation and magnitude change and corresponding histograms of the inverse calculation in study I in the dipole source space for the radial and tangential dipoles. The dipole shift is given in mm and the orientation change in degree. Note, that the scale of the color map of the values for magnitude change is not equidistant for values below and above one. The histograms of the magnitude change analysis show the relative magnitude change value according to (6).

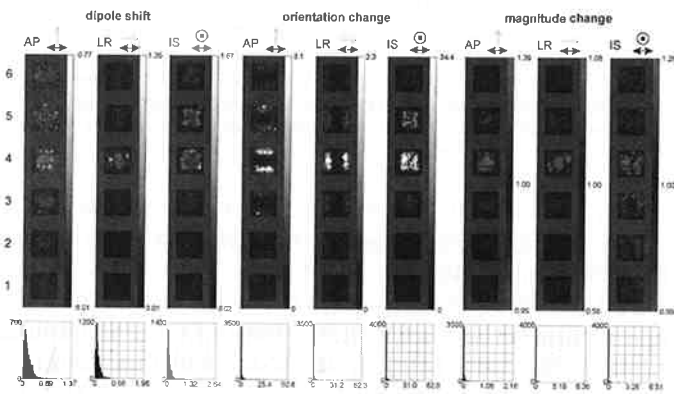


Fig. 6. Mapping of the analysis and corresponding histograms of the inverse calculation in study II in the dipole source space for the radial and tangential dipoles. The dipole shift is given in mm and the orientation change in degree. Note, that the color map of the values for magnitude change is not equidistant for values below and above one. The histograms of the magnitude change analysis show the relative magnitude change value according to (6).

cube (cf. Fig. 2). These maps clearly demonstrate an influence of anisotropy for the lower planes (4–6), similar to the forward computation (Fig. 4). For the upper planes the effect is less pronounced. For the dipole shift we obtained values up to 2.64 mm. However, in general the mean dipole shift was found to be very small. The influence on the orientation change was found to be significant at the edge of the anisotropic cube in case of dipoles oriented in AP and LR direction and centered below the cube in case of a IS dipole orientation.

C. Influence of Distance

To investigate the influence of the distance between the dipoles and the anisotropic structure we merged the results for AP, LR, and IS dipoles and grouped them by their distance to the anisotropy. The mean and variance for RDM^* , MAG_{rel} , dipole shift, relative magnitude change and orientation change were computed according to (9) and (10) and are displayed in Fig. 7. In addition, we considered the upper (1–3) and lower (4–6) planes separately. Fig. 7 clearly demonstrates that all values of all investigated quantities decrease with increasing

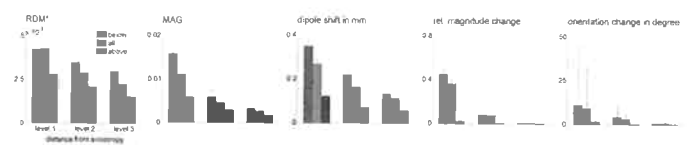


Fig. 7. Analysis of the influence of the distance on RDM^* , MAG , dipole shift, relative magnitude change and orientation change for results of study II. The diagrams show the mean value with variance obtained by assuming a Rayleigh distribution. Note that the variances for RDM^* and MAG are too small to be visible. Level 1–3 indicates the different layers with respect to the anisotropic cube. The results are given for all (green), the upper (blue) levels 1, 2, 3 and lower (red) levels 4, 5, 6.

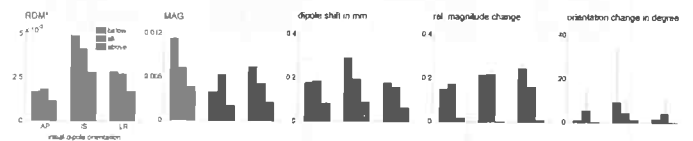


Fig. 8. Analysis of the influence of the original dipole orientation on RDM^* , MAG , dipole shift, relative magnitude change and orientation change for results of study II. The diagrams show the mean value with variance obtained by assuming a Rayleigh distribution. Note that the variances for RDM^* and MAG are too small to be visible. AP (anterior-posterior), LR (left-right), and IS indicate the different original dipole orientation according to Fig. 2. The results are given for all (green), the upper (blue), and lower (red) levels.

distance. The values for MAG_{rel} and relative magnitude change show a stronger decreases (more than linear) with distance as compared to RDM^* , dipole shift and orientation change. Furthermore, it is shown that in all cases the values for the planes below (4–6) the anisotropic cube are influenced more than the values of the planes above (1–3), which is also visible in Figs. 4 and 6.

D. Influence of Original Dipole Orientation

Fig. 8 displays the same data as Fig. 7, but this time grouped with respect to the three original dipole orientations (Fig. 2). Again the planes above and below the cube are considered separately. The results depicted in Fig. 8 are heterogeneous. There seems to be no prevailing configuration of dipole orientation versus anisotropy orientation producing larger or smaller errors than any other. Intuitively, we expected that positions below the anisotropy are influenced most strongly. However, in almost the half of the cases [$RDM^*(AP)$, $MAG(IS)$, dipole shift (AP), rel. magnitude change (AP, IS), and orientation change (AP, LR)] the mean value of all dipoles was found to be higher than for the dipoles at the planes below the cube.

E. Regions of Strong Influence

Fig. 9 shows a qualitative analysis of the above results, which was realized by employing 3-D models. From the upper 20% of the distribution of each calculated quantity we created, following three dimensional smoothing (Gaussian kernel with a width of 5.4 mm), an isosurface and visualized it along with the anisotropic cube. Table I lists the corresponding threshold values to the 0.8 percentile used in Fig. 9.

The strongest influence of anisotropy on RDM^* was found above the edges of the cube for dipoles in AP and LR orientation, which differs from the result for the IS orientation. The MAG_{rel} values are most strongly influenced if the dipole is oriented parallel to the surface of the anisotropic cube. We obtained very similar results for the relative magnitude change. Thus, the

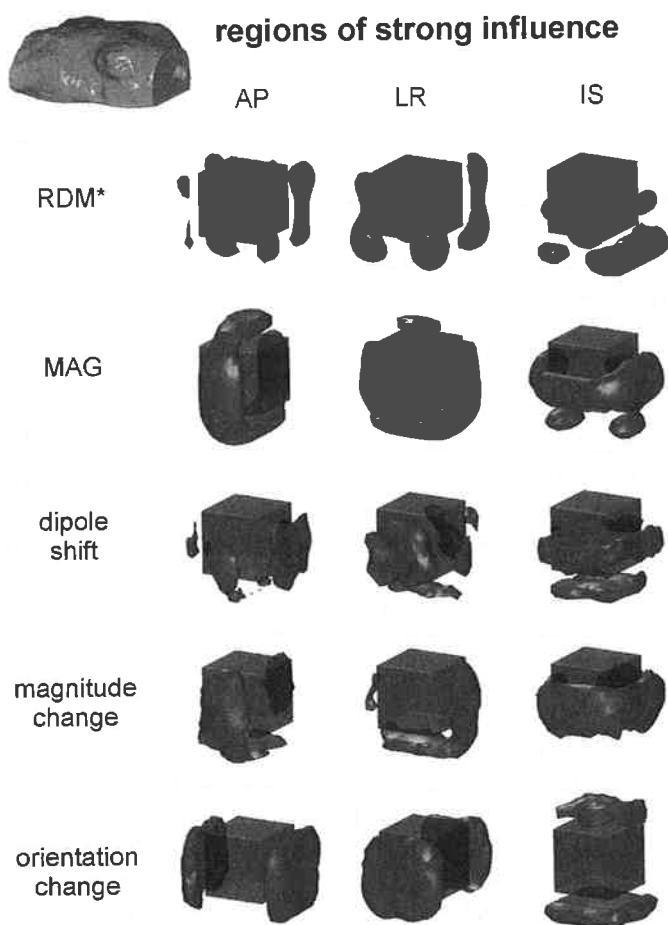


Fig. 9. Visualization of regions of strong influence when neglecting the anisotropy information in *study II*. The matrix of 3-D models shows the anisotropic cube in transparent blue, and regions of values above the 0.8 percentile for RDM*, MAG, dipole shift, magnitude change and orientation change are visualized by red surfaces. The isosurface model of the rabbit head in the upper left corner indicates the orientation of 3-D models.

TABLE I
THRESHOLD VALUES CORRESPONDING TO THE 0.8 PERCENTILE USED IN FIG. 9

	AP	LR ₀	IS
RDM*	0.0022	0.0039	0.0055
MAG _{rel}	0.0063	0.0047	0.0064
dipole shift in mm	0.24	0.19	0.20
relative magnitude change	0.035	0.023	0.035
orientation change in degree	1.04	0.82	0.68

MAG values of the forward computations predict quite well the results of the dipole magnitude changes in the inverse computations. On the contrary, the correlation between dipole shift and RDM* was found to be rather low, indicating that RDM* is not well predicting the dipole shifts. One reason for this might be due to the rather small values obtained for the dipole shift. The change of orientation was influenced most strongly for dipoles oriented perpendicular to the surface of the anisotropic cube.

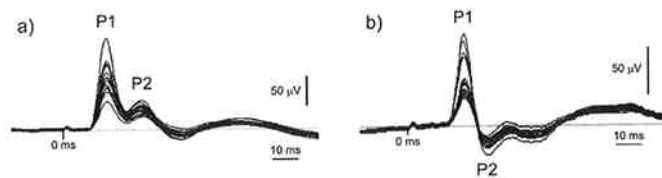


Fig. 10. Source localization based on ECoG recordings resulting from stimulation of the median nerve (a) and tibial nerve (b). Subfigure (c) shows the results employing a BEM model, (d) shows the estimated dipoles using the isotropic FEM model and (e) indicates the solution derived by using the anisotropic FEM model. The red dipoles are the results for the median nerve and the blue dipoles for the tibial nerve stimulation. Note, that the distance of the dipole positions is not clearly visible in both FEM models, since they are located below the cortical surface and a transparent visualization was not suitable as in the case of the BEM model.

F. Source Localization From Measurements

We performed source localization for the time instant of the first peak (Fig. 10), which is known to be generated in the somatosensory cortex S1. The latency of this peak after median nerve stimulation was 17.5 ms and 22 ms for the tibial nerve. The electric potential pattern was monopolar. In all inverse solutions (BEM, FEM isotropic, FEM anisotropic) the dipoles were found with slight differences in orientation and magnitude. The spatial difference in the dipole localization for both nerves averages to 2.0 mm (2.00 mm for the BEM, 1.89 mm for the isotropic FEM and 2.12 mm for the anisotropic FEM). This difference matches the expected anatomical difference of 2 mm. Moreover, the localized sources were within an accuracy of 1 mm in the expected cortical areas derived from anatomy. Fig. 10 also displays the result of the crosscheck between BEM and FEM based source localization (compare BEM and FEM isotropic). The dipole location difference between these two models was 0.42 mm for the tibial nerve and 0.51 mm for the median nerve stimulation. The dipole location difference between the results obtained with the anisotropic and the isotropic FEM model was 0.76 mm for the median nerve and 0.17 mm for the tibial nerve stimulation.

IV. DISCUSSION

In the present study, we investigated the influence of anisotropic conductivity on the forward and inverse computation in EEG experiments by applying a high-resolution FEM model of a rabbit head. Although FEM models permit the inclusion of anisotropy, this information has been rarely used in EEG source localization in the past due to the calculation and memory expense. Nowadays, the availability of affordable high-performance computing equipment and the recent development of fast and efficient solvers allow extensive studies in an acceptable time.

We found a strong influence of the anisotropy on the magnitude in the forward as well as in the inverse solution and on the orientation of dipoles in the inverse solution. On average, dipole shifts due to the anisotropy were within the limits of the procedural accuracy of EEG source localization. However, about 2% of the dipoles exhibited localization errors significantly higher than the procedural limit. The low localization errors and the relatively high magnitude changes are in good agreement with the results of Haueisen *et al.* [7]. Furthermore, anisotropy in the innermost layer of a four layer spherical volume conductor had a strong effect on the magnitude of the electric potential produced

by a tangential dipole, but only a weak effect on the topology [36]. However, the presented results reflect only the influence of neglecting anisotropy information in the used model. There are further modeling errors which can lead to significant changes of the forward as well as inverse solution. Slight changes of the tissue conductivity next to the source, would affect the results significantly [37], [38] as would a neglect of parts of the model as shown by He *et al.* [39]. These modeling errors would superimpose the effect of neglecting anisotropy.

In contrast to the low RDM* values for single dipoles found in study II, a briefly tested setup of multiple dipoles (*study III*) showed significantly higher RDM* values (up to 4 times). However, we found also that the RDM* could be lower compared to a single dipole (based on the values obtained for the three dipoles in *study II*). Since the investigation of multiple dipoles can lead to a vast number of combinations, a general conclusion from this limited test cannot be drawn. Nevertheless, it shows that neglecting an anisotropic conductivity can strongly extend the error in the forward solution using multiple dipoles.

A clear result of the presented *studies I* and *II* was that all investigated result measures (RDM*, MAG, shift, magnitude, and orientation change) were more strongly influenced the closer the dipoles were placed to the anisotropy. Consequently, we would expect a stronger influence on all quantities if the dipoles would be located inside the anisotropic tissue. RDM* and dipole shift seem to be more linearly dependent on the distance between dipole and anisotropy, whereas, MAG, magnitude and orientation changes seem to be nonlinearly correlated to this distance.

One further result of our *study II* was that all investigated result measures were influenced stronger for planes below the cube than for planes above. This is in principal agreement with Anwander *et al.* [14] and Wolters *et al.* [15], [16]. Despite the three exceptions visible (see Fig. 9), our result measures seem to be less affected when the dipoles are positioned above the anisotropic cube. Such a setting is actually the most common for animal studies in rabbit or rat, because of their lissencephalic brain. Also, in the human brain such a geometrical situation is common for the crown of a gyrus.

As presented in Figs. 8 and 9 of *study II*, the relation between the orientation of the dipole and the orientation of the anisotropy seems to have little influence on the estimated dipole orientation and magnitude when neglecting anisotropy. In other words, the influence of anisotropy seems not to be dependent on the direction of the dipole orientation relative to the anisotropy orientation, but on the dipole direction relative to the cube as such. If the dipoles point perpendicular to the cube the influence is less than if they point parallel to the cube. Since the orientation of the dipole was strongly influenced by the anisotropy in the inverse computation, we would expect a correlation between the orientation of the dipole and the anisotropy orientation. However, the results reflect that the anisotropic block as such has more influence on the reconstructed orientation than the relation between the orientation of the dipole and the orientation of the anisotropy. As an experimental confirmation for this observation we can consider at least in part the results by Liehr and Haueisen [40]. They investigated by using magnetic measurements in a physical phantom a variety of dipole orientations relative to anisotropy orientations and found that for dipoles both at 0° and 90° the orientation error was minimal. The cor-

responding magnitude changes, however, are not directly comparable to our results since their dipolar source was located within the anisotropic material. Nevertheless, the tendency that the 0 degree setup (in our case: LR) has lower MAG values and relative magnitude change values is also seen in our data (Table I). A setup with dipoles within the anisotropic material cannot be modeled with our current software and will be investigated in future studies.

Fig. 9 indicates a negative correlation between the magnitude and orientation change (strong changes in orientation correlate with weak changes in magnitude and vice versa). This is, however, true only for the largest 20% of the values presented in this figure. For smaller values, there is a positive correlation between both result measures, also independent of the orientation of the dipoles.

The distribution (relative occurrence) of the result measures was found to be clearly non-Gaussian, whereas a Rayleigh distribution fitted the data well. Visually similar distributions were observed in a recent simulation study with a spherical head model including anisotropy [41].

In the localization study with values taken from real measurements (SEP after stimulation of median and tibial nerve, DTI derived conductivity data of the rabbit white matter) we employed three different volume conductor models (BEM, isotropic and anisotropic FEM). We found comparable results with all three models: the localization was in agreement with the anatomical expectation and the distance between the two dipoles (median and tibial nerve) was also as anatomical expected. These results both verify the modeling approach itself and are consistent with the above discussed relatively small influence found in the simulations of dipoles located above a white matter tract. The distance between our simulated dipole layers and the anisotropic cube (*study II*) represents a typical anatomical distance for the rabbit brain [42].

Finally, we conclude that source localization procedures in animals will improve when including white matter anisotropy information. This holds for dipole orientation and magnitude estimations more than for dipole localizations. The influence of anisotropy on source estimation was found to be complex. Therefore, a direct transfer of our results to other species (including humans) has to be considered with caution.

REFERENCES

- [1] L. A. Geddes and L. E. Baker, "The specific resistance of biological material—a compendium of data for the biomedical engineer and physiologist," *Med. Biol. Eng.*, vol. 5, no. 3, pp. 271–293, May 1967.
- [2] P. W. Nicholson, "Specific impedance of cerebral white matter," *Exp. Neurol.*, vol. 13, no. 4, pp. 386–401, Dec. 1965.
- [3] Y. C. Okada, J. C. Huang, M. E. Rice, D. Tranchina, and C. Nicholson, "Origin of the apparent tissue conductivity in the molecular and granular layers of the *in vitro* turtle cerebellum and the interpretation of current source-density analysis," *J. Neurophysiol.*, vol. 72, no. 2, pp. 742–753, Aug. 1994.
- [4] C. Polk and E. Postow, Eds., *CRC Handbook of Biological. Effects of Electromagnetic Fields* Boca Raton, FL, CRC Press, 1986.
- [5] J. B. Ranck, "Specific impedance of rabbit cerebral cortex," *Exp. Neurol.*, vol. 7, pp. 144–152, 1963.
- [6] A. van Harreveld, T. Murphy, and K. W. Nobel, "Specific impedance of rabbit's cortical tissue," *Am. J. Physiol.*, vol. 205, pp. 203–207, 1963.
- [7] J. Haueisen, D. S. Tuch, C. Ramon, P. H. Schimpf, V. J. Wedeen, J. S. George, and J. W. Belliveau, "The influence of brain tissue anisotropy on human EEG and MEG," *NeuroImage*, vol. 15, no. 1, pp. 159–166, Jan. 2002.

- [8] D. S. Tuch, V. J. Wedeen, A. M. Dale, J. S. George, and J. W. Belliveau, "Conductivity tensor mapping of the human brain using diffusion tensor MRI," *Proc. Nat. Acad. Sci. USA*, vol. 98, no. 20, pp. 11697–11701, Sep. 2001.
- [9] Y. Yan, P. L. Nunez, and R. T. Hart, "Finite-element model of the human head: scalp potentials due to dipole sources," *Med. Biol. Eng. Comput.*, vol. 29, no. 5, pp. 475–481, Sep. 1991.
- [10] M. Thevenet, O. Bertrand, F. Perrin, T. Dumont, and J. Pernier, "The finite element method for a realistic head model of electrical brain activities: preliminary results," *Clin. Phys. Physiol. Meas.*, vol. 12 Suppl A, pp. 89–94, 1991.
- [11] N. G. Sepulveda, C. F. Walker, and R. G. Heath, "Finite element analysis of current pathways with implanted electrodes," *J. Biomed. Eng.*, vol. 5, no. 1, pp. 41–48, Jan. 1983.
- [12] C. E. Miller and C. S. Henriquez, "Finite element analysis of bioelectric phenomena," *Crit. Rev. Biomed. Eng.*, vol. 18, no. 3, pp. 207–233, 1990, Review.
- [13] G. Marin, C. Guerin, S. Baillet, L. Gamero, and G. Meunier, "Influence of skull anisotropy for the forward and inverse problem in EEG: simulation studies using FEM on realistic head models," *Hum. Brain. Mapp.*, vol. 6, no. 4, pp. 250–269, 1998.
- [14] A. Anwander, C. H. Wolters, M. Dümpelmann, and T. Knösche, "Influence of realistic skull and white matter anisotropy on the inverse problem in EEG/MEG-source localization," in *Proc. 13th Int. Conf. Biomagnetism*, 2002, pp. 679–681.
- [15] C. H. Wolters, A. Anwander, X. Tricoche, S. Lew, and C. R. Johnson, "Influence of local and remote white matter conductivity anisotropy for a thalamic source on EEG/MEG field and return current computation," *Int. J. Bioelectromagn.*, vol. 7, no. 1, May 2005.
- [16] C. H. Wolters, A. Anwander, X. Tricoche, D. Weinstein, M. A. Koch, and R. S. MacLeod, "Influence of tissue conductivity anisotropy on EEG/MEG field and return current computation in a realistic head model: a simulation and visualization study using high-resolution finite element modeling," *NeuroImage*, 2005, to be published.
- [17] D. Güllmar, J. R. Reichenbach, A. Anwander, T. Knösche, C. H. Wolters, M. Eiselt, and J. Hauelsen, "Influence of anisotropic conductivity of the white matter tissue on EEG source reconstruction—a FEM simulation study," *Int. J. Bioelectromagn.*, vol. 7, no. 1, May 2005.
- [18] L. Flemming, Y. Wang, A. Caprihan, M. Eiselt, J. Hauelsen, and Y. C. Okada, "Evaluation of the distortion of EEG signals caused by a hole in the skull mimicking the fontanel in the skull of human neonates," *Clin. Neurophysiol.*, vol. 116, no. 5, pp. 1141–1152, 2005.
- [19] M. Eiselt, F. Giessler, D. Platzek, J. Hauelsen, U. Zwiener, and J. Rother, "Inhomogeneous propagation of cortical spreading depression-detection by electro- and magnetoencephalography in rats," *Brain Res.*, vol. 1028, no. 1, pp. 83–91, 2004.
- [20] S. M. Bowyer, N. Tepley, N. Papuashvili, S. Kato, G. L. Barkley, K. M. Welch, and Y. C. Okada, "Analysis of MEG signals of spreading cortical depression with propagation constrained to a rectangular cortical strip. II. Gyrencephalic swine model," *Brain Res.*, vol. 843, no. 1–2, pp. 79–86, 1999.
- [21] S. M. Bowyer, Y. C. Okada, N. Papuashvili, J. E. Moran, G. L. Barkley, K. M. Welch, and N. Tepley, "Analysis of MEG signals of spreading cortical depression with propagation constrained to a rectangular cortical strip. I. Lissencephalic rabbit model," *Brain Res.*, vol. 843, no. 1–2, pp. 71–78, 1999.
- [22] U. G. Nolte, J. Finsterbusch, and J. Frahm, "Rapid isotropic diffusion mapping without susceptibility artifacts: whole brain studies using diffusion-weighted single-shot STEAM MR imaging," *Magn. Reson. Med.*, vol. 44, no. 5, pp. 731–736, Nov. 2000.
- [23] Statistical Parametric Mapping (2005) 2005 [Online]. Available: <http://www.fil.ion.ucl.ac.uk/spm/spm2.html>
- [24] P. Basser, J. Mattiello, and D. LeBihan, "MR diffusion tensor spectroscopy and imaging," *Biophys. J.*, vol. 66, pp. 259–267, 1994.
- [25] J. S. Shimony, R. McKinstry, E. Akbudak, J. A. Aronovitz, A. Z. Snyder, N. F. Lori, T. S. Cull, and T. E. Conturo, "Quantitative diffusion-tensor anisotropy brain MR imaging: Normative human data and anatomical analysis," *Radiology*, vol. 212, pp. 770–784, 1999.
- [26] C. H. Wolters, M. Kuhn, A. Anwander, and S. Reitzinger, "A parallel algebraic multigrid solver for finite element method based source localization in the human brain," *Comp. Vis. Sci.*, vol. 5, no. 3, pp. 165–177, 2002.
- [27] P. H. Schimpf, C. Ramon, and J. Hauelsen, "Dipole models for the EEG and MEG," *IEEE Trans. Biomed. Eng.*, vol. 49, no. 5, pp. 409–418, May 2002.
- [28] H. Buchner, G. Knoll, M. Fuchs, A. Rienäcker, R. Beckmann, M. Wagner, J. Silny, and J. Pesch, "Inverse localization of electric dipole current sources in finite element models of the human head," *Electroencephalogr. Clin. Neurophysiol.*, vol. 102, pp. 267–278, Apr. 1997.
- [29] M. Mohr and B. Vanrumste, "Comparing iterative solvers for linear systems associated with the finite difference discretization of the forward problem in electro-encephalographic source analysis," *Med. Biol. Eng. Comp.*, vol. 41, pp. 75–84, 2003.
- [30] C. H. Wolters, L. Grasedyck, and W. Hackbusch, "Efficient computation of lead field bases and influence matrix for the FEM-based EEG and MEG inverse problem," *Inverse Prob.*, vol. 20, no. 4, pp. 1099–1116, Aug. 2004.
- [31] N. G. Gencer and C. E. Acar, "Sensitivity of EEG and MEG measurements to tissue conductivity," *Phys. Med. Biol.*, vol. 49, no. 5, pp. 701–717, Mar. 2004.
- [32] "SimBio project (1999–2003)," A Generic Environment for Bionumerical Simulation. IST Programme Framework V Project IST-1999-10378 [Online]. Available: <http://www.simbio.de>
- [33] A. Anwander and C. H. Wolters, NeuroFEM Software 2000–2005 [Online]. Available: <http://www.neurofem.com>
- [34] J. W. H. Meijis, O. W. Weier, M. J. Peters, and A. van Oosterom, "On the numerical accuracy of the boundary element method," *IEEE Trans. Biomed. Eng.*, vol. 36, no. 10, pp. 1038–1049, Oct. 1989.
- [35] M. S. Hämäläinen and J. Sarvas, "Realistic conductivity geometry model of the human head for interpretation of neuromagnetic data," *IEEE Trans. Biomed. Eng.*, vol. 36, no. 2, pp. 165–171, Feb. 1989.
- [36] H. Zhou and A. van Oosterom, "Computation of the potential distribution in a four layer anisotropic concentric spherical volume conductor," *IEEE Trans. Biomed. Eng.*, vol. 39, no. 2, pp. 154–158, Feb. 1992.
- [37] J. Hauelsen, C. Ramon, M. Eiselt, H. Brauer, and H. Nowak, "Influence of tissue resistivities on neuromagnetic fields and electric potentials studied with a finite element model of the head," *IEEE Trans. Biomed. Eng.*, vol. 44, no. 8, pp. 727–735, Aug. 1997.
- [38] K. A. Awada, D. R. Jackson, S. B. Baumann, J. T. Williams, D. R. Wilton, P. W. Fink, and B. R. Prasky, "Effect of conductivity uncertainties and modeling errors on EEG source localization using a 2-D model," *IEEE Trans. Biomed. Eng.*, vol. 45, no. 9, pp. 1135–1145, Sep. 1998.
- [39] B. He, T. Musha, Y. Okamoto, S. Homma, Y. Nakajima, and T. Sato, "Electric-Dipole tracing in the brain by means of the boundary element method and its accuracy," *IEEE Trans. Biomed. Eng.*, vol. 34, no. 6, pp. 406–414, Jun. 1987.
- [40] M. Liehr and J. Hauelsen, "Experimentally observed influence of anisotropic compartments in a volume conductor on the magnetic field distribution generated by artificial current dipoles," *Int. J. Bioelectromagn.*, vol. 7, no. 1, May 2005.
- [41] H. Hallez, B. Vanrumste, P. van Hesel, Y. d'Asseler, I. Lemahieu, and R. van de Walle, "A finite difference method with reciprocity used to incorporate anisotropy in electroencephalogram dipole source localization," *Phys. Med. Biol.*, vol. 50, pp. 3787–3806, Aug. 2005.
- [42] H. J. Gould, 3rd, "Body surface maps in the somatosensory cortex of rabbit," *J. Comp. Neurol.*, vol. 243, no. 2, pp. 207–233, Jan. 1986.



Daniel Güllmar received the diploma in media technology from the Technical University Ilmenau, Ilmenau, Germany, in 2001. Since 2002, he is working towards the Ph.D. degree at the Institute of Diagnostic and Interventional Radiology and at the Biomagnetic Center, both assigned to the Friedrich-Schiller-University, Jena, Germany.

His research interests are in conductivity tensor imaging based on diffusion tensor imaging to include anisotropy information in the conductor model which were used in EEG/MEG source localization.



Jens Hauelsen (M'03) received the M.S. and Ph.D. degrees in electrical engineering from the Technical University Ilmenau, Ilmenau, Germany, in 1992 and 1996, respectively.

From 1996 to 1998, he worked as a Postdoc and from 1998 to 2005 as the head of the Biomagnetic Center, Friedrich-Schiller-University, Jena, Germany. Since 2005, he is Professor of Biomedical Engineering and directs the Institute of Biomedical Engineering and Informatics at the Technical University Ilmenau. His research interests are in

the numerical computation of bioelectromagnetic fields and the analysis of bioelectromagnetic signals.



Michael Eiselt was born in Gera, Germany, in 1956. He received the M.D. degree in 1983, the Ph.D. degree in 1987, and the specialization in pathophysiology in 1987.

He is presently a Research Associate at the Medical Faculty of the Friedrich Schiller University, Jena, Germany. His research interests include clinical and experimental neuropathophysiology with special regards to dysfunctions during early human development. Since 1991, he performed the investigations using MEG and EEG/ECOG.



Frank Gießler received the Ph.D. degree in physics from the Friedrich-Schiller-University Jena, Jena, Germany in 1991.

After a one-year stay at the Institute of Biomedical Engineering of the Tampere University of Technology, Tampere, Finland, he rejoined the Biomagnetic Center in Jena as a Scientist. His interests are in MEG instrumentation and measurements of small volume objects.



Lars Flemming graduated from Medical School of the Friedrich-Schiller-University of Jena, Jena, Germany, in 2000. From 2000 until 2003 he worked at the same university as a Scientist at the Biomagnetic Center and at the Biomedical Research and Integrative NeuroImaging (BRaIN Imaging) center of the University of New Mexico, Albuquerque, NM. Since 2003, he is a Resident of Surgery at the hospital "Kantonsspital Aarau," Switzerland. EEG/MEG source localization and neuroimaging are his scientific interests.



Alfred Anwander received the M.Sc. degree in electrical engineering from the University of Karlsruhe, Karlsruhe, Germany, in 1996, and M.Sc. (DEA) and Ph.D. degrees from INSA Lyon Scientific and Technical University of Lyon, Lyon, France, in 1996 and 2001, respectively.

Since 2000 he is Scientist at the Max Planck Institute for Human Cognitive and Brain Sciences, Leipzig, Germany. His research interests are in EEG/MEG source localization and quantitative connectivity from diffusion MRI.



Thomas R. Knösche received the M.S. degree in electrical engineering from the Technical University Ilmenau, Ilmenau, Germany, in 1992. He received the Ph.D. degree in applied physics from the University of Twente, Twente, The Netherlands, in 1996.

From 1993 to 1995 he worked as a research assistant at the University of Twente. From 1996 to 1998, he worked as a Postdoc at the Max-Planck-Institute of Cognitive Neuroscience, Leipzig, Germany, and from 1999 to 2001 as Research & Development Manager at A.N.T Software B.V., Enschede, Netherlands.

Since 2001 he is Research Scientist at the Max-Planck-Institute of Human Cognitive and Brain Sciences. His research interests include the reconstruction of the generators of neuroelectromagnetic fields, the analysis of diffusion weighted magnetic resonance images, and the neurocognition of music.



Carsten H. Wolters studied in Aachen, Germany and Lyon and Paris, France and received the M.Sc. degree (*summa cum laude*) in applied mathematics with a minor in medicine from the RWTH, Aachen, in 1997. He carried out his diploma thesis at RWTH Aachen developing the FEM-based EEG/MEG inverse problem software toolbox CAUCHY. He received the Ph.D. degree (*magna cum laude*) from the Faculty of Mathematics and Computer Science, University of Leipzig, Leipzig, Germany, on the influence of inhomogeneities and anisotropies on EEG/MEG source reconstruction in 2003.

During the school-year 1992-1993, he started working in the field of BEM modeling for EEG source analysis at INSERM-U 280 in Lyon. After his diploma, he moved to Leipzig/Germany and founded a cooperative project between the MEG group of the Max-Planck Institute (MPI) for Human Cognitive and Brain Sciences and the MPI for Mathematics in the Sciences. He was a Principal Investigator of the large scale European project SimBio, in which the source reconstruction software IP-NeuroFEM was developed. In February 2004, he joined the Scientific Computing and Imaging Institute at the University of Utah. Since March 2005, he is a Research Associate at the Institute for Biomagnetism and Biosignalanalysis at the University of Münster, Münster, Germany. His research interests are in the field of neurosciences: EEG and MEG inverse methods, realistic anisotropic high-resolution FE head modeling, DTI and EIT, image registration and segmentation, and signal processing.



Matthias Dümpelmann was born in Germany, in 1963. He received the degree in electrical engineering in 1988 and the Ph.D. degree in 1998, both from the Department of Electrical Engineering at the Ruhr-Universität-Bochum, Germany. Between 1988 and 2000 he worked at the university hospitals of Bonn in the clinic for epilepsy. Main focus of his research work was the analysis and detection of epileptiform transients in EEG recordings. He joined ANT Software/eemagine Medical Imaging Solutions (Enschede, Netherlands and Berlin, Germany) as a Scientific Developer in 2000. His current research and development work covers signal processing of biomedical signals, source localization methods based on EEG or MEG recordings, and medical image processing.

His current research and development work covers signal processing of biomedical signals, source localization methods based on EEG or MEG recordings, and medical image processing.



David S. Tuch He received the B.A. degree in physics from the University of Chicago, Chicago, IL, and the Ph.D. degree from the Harvard-Massachusetts Institute of Technology (M.I.T.) Division of Health Sciences and Technology and the MIT Department of Nuclear Science and Engineering, Cambridge, MA.

While at M.I.T., he was a graduate Research Assistant in the Los Alamos National Laboratory, Biophysics Group, Los Alamos, NM. He is an Instructor of Radiology at Harvard Medical School and an Assistant in Physics at Massachusetts General Hospital. He completed a Postdoctoral Fellowship at Massachusetts General Hospital, Harvard Medical School. His research interests include diffusion-weighted MRI, imaging of biotransport, and statistical image analysis.



Jürgen R. Reichenbach received the M.S. and Ph.D. degrees in physics from the University of Karlsruhe, Karlsruhe, Germany, in 1988 and 1992, respectively.

In 1993, he worked as a Postdoctoral Fellow at the University of Montpellier, Montpellier, France and in 1994 at the Heinrich-Heine University, Düsseldorf, Germany. Following two years as a Visiting Associate Scientist at the Mallinckrodt Institute of Radiology, St. Louis, MO, he joined the Friedrich-Schiller-University, Jena, Germany. He heads a research team working on the development

of new measurement techniques in the field of magnetic resonance imaging (MRI).